Effect of Surface Chemistry on Electronic Properties of Carbon Nanotube Network Thin Film Transistors

Michael Vosgueritchian, Melburne C. LeMieux, Daniel Dodge, and Zhenan Bao*

Department of Chemical Engineering, Stanford University, Stauffer III, 381 North-South Mall, Stanford, California 94305-5025

ABSTRACT   Thin films of single-walled carbon nanotubes (SWNTs) are a viable nanomaterial for next generation sensors, transistors, and electrodes for solar cells and displays. Despite their remarkable properties, challenges in synthesis and processing have hindered integration in current electronics. Challenges include the inability to precisely assemble and control the deposition of SWNT films on a variety of surfaces and the lack of understanding of the transport properties of these films. Here, we utilize an optimized "dry transfer" technique that facilitates the complete intact transfer of SWNT films between different surfaces. We then show the effect of surface chemistry on the electronic properties of SWNT films. By isolating the effect of the surface, we gain insight into the fundamental transport properties of SWNTs on surfaces with different chemical functionalities. Thin film transistor (TFT) characteristics, corroborated with μ-Raman spectroscopy, show that by using different surface chemical functionalities it is possible to alter the electronic properties of SWNT films. This opens up another route to tune the electronic properties of integrated SWNT films.

KEYWORDS: carbon nanotube network · self-assembled monolayer · nanotube/surface interactions · nanotube transport properties · carbon nanotube transistor

Single-walled carbon nanotubes (SWNTs) have attracted intense research effort due to their excellent electrical, mechanical, optical, and thermal properties.[1,2] A wide variety of applications are possible using these nanomaterials in devices including displays,[3] touch screens, flexible electronics,[4] and as electrodes in photovoltaics.[5] In addition, due to their unique 1D structure and large surface area, they can be used as the active material in efficient, disposable sensors.[6−10] However, despite great potential, SWNTs have yet to be utilized in practical electronic devices. This is mainly due to several fundamental issues in synthesis and processing, including (1) the electrical heterogeneity of SWNTs, in which the electronic properties depend on the chirality and diameter of the nanotubes, and (2) the inability to reproducibly control the alignment, density, and direct assembly on different surfaces from solution.

These limitations, manifested as slight deviations in the reproducibility of film morphology, can dramatically alter the electronic properties of SWNT films.[11] The former issue can be mitigated by using thin films of SWNTs in the form of random networks, which average the electrical heterogeneity of the individual nanotubes and, in addition, increase the current carrying capacity. However, in this case, it is difficult to clearly understand and decouple variables that affect charge transport. While easily fabricated, thin films of randomly aligned networks assembled from solution pose several problems. First, these films are composed of metallic, semi-metallic, and semiconducting nanotubes, which lead to ambiguous electronic response and unreliable devices.[12] As a result, substantial effort has been focused on growing single chiral-

ity SWNTs using chemical vapor deposition[13] or bulk separation methods such as selective reactions[14] and density gradient centrifugation.[15] Significant progress has been achieved using these methods, but further development is required for a better yield and more consistent electronic performance in SWNT films. Second, the lack of alignment increases tube junctions between crossing SWNTs, causing large current loss due to high contact resistance at these points.[16,17] Alignment increases density while keeping tube junctions low, although a certain level of misalignment is necessary in order for the SWNTs to form a percolating network.[18] Several different methods have been developed to deal with the alignment issue, including CVD growth of SWNTs on quartz substrates,[19] dielectrophoresis,[20] surface patterning,[21] and Langmuir−Blodgett deposition.[22]

The solution deposition of SWNT networks on a substrate is aided by surface treatment for the SWNTs to adsorb. It is

unclear what the effects of such surfaces are on the charge transport of SWNTs. Thus, a fundamental understanding of SWNT charge transport is still needed. Recently, we have shown controlled alignment, deposition, and sorting of SWNT networks through spin-assembly.[23] This methodology also has the added advantage that it does not require high-temperature processing steps and thus enables the use of flexible plastic substrates.[24] While this process led to organized SWNT networks with reliable electronic properties, it is only applicable on select surfaces due to poor solvent wetting and weak surface/SWNT interaction on other surfaces. In a recent study, we examined the nature of the adsorption of SWNTs on amine-functionalized surfaces.[25] With this in mind, it would be interesting to see the effects of different substrate surface chemistry on the electronic properties of SWNT networks. It has been shown that different self-assembled monolayers (SAMs) have a significant impact on the electrical properties of organic thin film transistors (TFTs), such as shifting the threshold voltage,[26,27] current−voltage hysteresis,[28] source−drain current, and field effect mobility.[29] These effects have been attributed to several factors including charge traps, doping, and surface dipoles. Limited analogous studies have investigated the effect of different substrate surface chemical functionalities on SWNT network field effect transistors (FETs).[30] SWNTs are ideal sensor materials since they are extremely responsive to their surroundings as they are completely composed of surface atoms, thus it is reasonable to expect that SWNT network electrical behavior will be manipulated through interactions with different moieties, as has been observed before.[31]
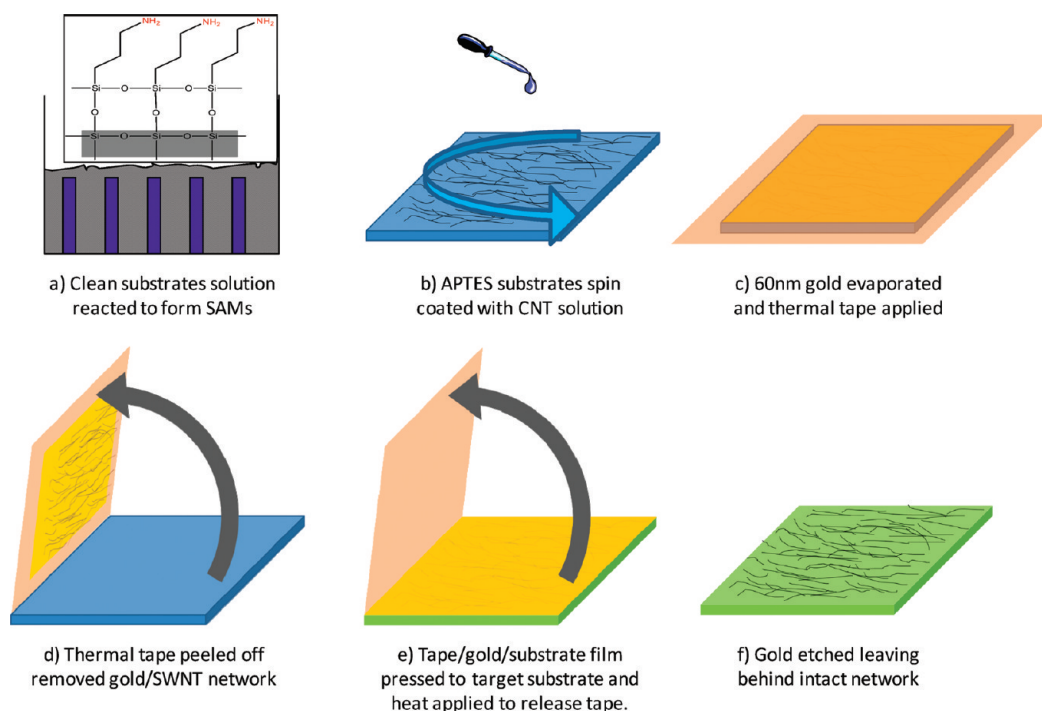
Here, we first utilize a dry transfer technique that can reliably transfer the spin-assembled SWNT networks intact (without changing alignment and density) between various surfaces. This critical step allowed the transfer to both hydrophobic and hydrophilic surfaces, enabling us to gain fundamental insights into the effect of dielectric surface modification on SWNT charge transport. Surface chemistry was altered through covalently immobilized SAMs with different functional terminal groups. We investigated the effects of SAMs with several different end functional groups, such as bromine, cyano, amine, and methyl, on SWNT FET properties. Our results show that surface chemistry has a significant impact on the mobility (μ), threshold voltage (V_t), source−drain currents (I_{on}), current−voltage hysteresis, and the ratio of the on-current to the off-current (on/off ratio) of the FETs. As a result, the electrical properties of SWNT-based FETs can be tuned using SAMs. This can potentially allow the design of novel devices such as memory devices, logic circuits, or sensors with increased specificity with the same SWNT films on different SAMs.

RESULTS AND DISCUSSION

SWNT Film Formation. A detailed description of our spin-assembly deposition of partially aligned and semiconductor-enriched SWNT network films can be found elsewhere[23,32] and in the Materials and Methods section. Briefly, solutions of arc-discharge SWNTs in n-methyl pyrrolidone (NMP) at 10 μg/mL were spin-coated on 3-aminopropyltriethoxysilane (APTES)-functionalized Si/SiO$_2$ substrate. Spin-coating conditions were optimized previously;[32] 150 μL of solution was deposited at 4000 rpm and then annealed at 150 °C for 1 h under vacuum to remove residual NMP. Atomic force microscopy (AFM) imaging confirmed partially aligned nanotubes with typical density of about 8−10 SWNTs/μm^2.

SWNT Film Transfer. As it is difficult to fabricate the same SWNT network film (same density, alignment, chirality) and compare on different surfaces, developing a reliable transfer method of the SWNT networks is critical to enable this study. Different methods have been reported for transferring SWNT films from one surface to another, including polydimethylsiloxane (PDMS) stamps,[33,34] poly(methyl methacrylate) (PMMA) films,[35] and thermally activated adhesive tapes.[36] After investigating a variety of methods, we concluded that the thermal adhesive tape method yields the best transfers for our substrates, while maintaining alignment and limiting contamination from the transfer process. First, a 60 nm layer of gold was evaporated on the SWNT donor substrate to assist with peeling off the SWNT network. The thermal tape was then applied onto the donor substrate and peeled off, removing with it the gold/SWNT film. The tape/gold/SWNT film was then pressed onto the acceptor substrate and heated to 120 °C to delaminate the thermal tape, leaving behind the gold/SWNT film; the gold film was subsequently etched away, leaving behind the SWNT network on the substrate (schematic of the process is shown in Scheme 1).

Several different SAMs with different terminal chemical functional groups were used. They were n-octadecyltrichlorosilane (OTS), 11-cyanoundecyltrimethoxysilane (CTS), and 11-bromoundecyltrimethoxysilane (BTS). SWNT films were also transferred to unfunctionalized surfaces of SiO$_2$ (bare) and another APTES surface prepared under identical conditions as those used to prepare the original SWNT films. The thickness, contact angle, and root-mean-square (rms) surface roughness (obtained from AFM) are given in Table 1. These results confirm that uniform and smooth monolayers were formed. AFM images (Figure 1) also confirmed that there was no loss of density or alignment of SWNTs during the transfer process. Yields for transfers to APTES, BTS, and CTS surfaces were typically around 100% as good adhesion was formed between the transferred film and the surface. Transfer to a bare SiO$_2$ or OTS surface was more difficult and required applying a higher pressure. This

Scheme 1. Device fabrication and transfer process using thermal tape.

a) Clean substrates solution reacted to form SAMs

b) APTES substrates spin coated with CNT solution

c) 60nm gold evaporated and thermal tape applied

d) Thermal tape peeled off removed gold/SWNT network

e) Tape/gold/substrate film pressed to target substrate and heat applied to release tape.

f) Gold etched leaving behind intact network

is most likely due to weak interaction between these surfaces and the SWNT film as SWNTs are adsorbed on the surface *via* van der Waals forces. As a result, slight changes in the alignment were observed on the bare surfaces. While 100% transfer was achieved onto the bare Si surface, a typical transfer to an OTS surface has a yield of about 25%. We attributed this to the extreme hydrophobicity of the surface which gives poor adhesion between the transferred films and the surface.

Electrical Properties. To understand the effect of the surface chemistry on the electrical properties, we fabricated top contact transistor devices from the SWNT films on the different SAMs. Gold was thermally evaporated through a shadow mask to deposit source/drain electrodes with a channel length (L_c) of 50 μm and width (W_c) of 1000 μm. The TFT characteristics were measured using a Keithley parameter analyzer. The data were averaged over 6−8 devices per sample and three samples per SAM. The exception is OTS, with only one sample tested, due to poor transfers. Average current−voltage (I−V) transfer plots are shown in Figure 2a, and output plots can be seen in the Supporting

Information. Comparisons between the average on-current (I_{on}), mobility (μ), on/off ratio, and threshold voltage (V_t) between the different SAMs is summarized in Figure 3.

Most notably, we observed a significant increase in I_{on} and μ for SWNTs transferred onto BTS surfaces compared to the other SAMs (an increase by a factor of 2). This is most likely due to the electron-withdrawing bromine group interacting with the SWNTs. Since semiconducting SWNTs are p-type in ambient air, electron-withdrawing bromine may induce positive charges in the SWNTs and increase the number of charge carriers (holes). This explains the increase in I_{on} and μ since they are directly proportional to the number of charge carriers. Increased conductivity in SWNTs has been observed before by directly doping SWNTs with p-type dopants such as bromine or $SOCl_2$.[31] However, in those cases, the dopant is typically unstable as the doping effect diminishes over time due to the volatile nature of these species, whereas our system provides a permanent alteration of charge transport of the SWNTs. In fact, the electrical values were consistent sixth months after the initial analysis and after annealing at 150 °C for over an hour under vacuum. Moreover, the results indicate that, despite the very small BTS/SWNT contact area, a significant impact of the SAM on the transport properties was still observed. All samples showed good transistor behavior with typical devices having on/off ratios of over 10^3. The other SAMs had less of an impact on charge transport compared to the BTS SAM. In addition to the lack of charge transfer, it is possible that increased hydrophilicity of the other SAMs could also

TABLE 1. Contact Angle Measured by Contact Angle Goniometer, Thickness Measured by Ellipsometry, and Root-Mean-Square (RMS) Roughness Measured by AFM for the Different SAMs

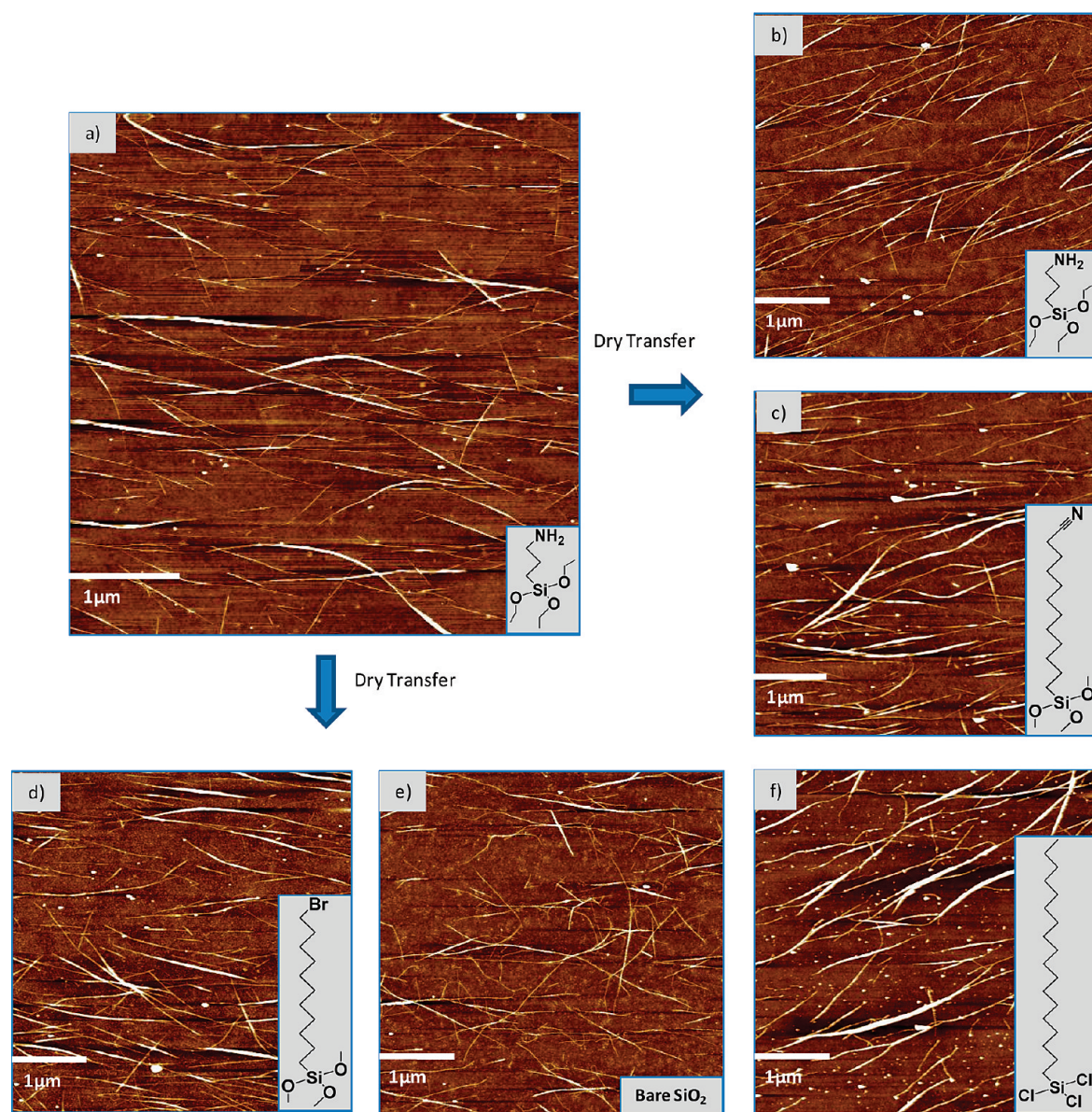| SAM	contact angle (deg)	thickness (Å)	rms (nm)
bare SiO$_2$	0	N/A	0.24
APTES	60	8	0.34
CTS	51	8	0.26
BTS	77	15	0.45
OTS	101	21	0.41

Figure 1. A 5 μm × 5 μm image with 10 nm Z scale AFM images of transfer samples of (a) original network on APTES, (b) transferred to APTES, (c) transferred to CTS, (d) transferred to BTS, (e) transferred to bare (SiO₂), and (f) transferred to OTS.

explain the decreased performance compared to the BTS, such as on the APTES and CTS surfaces, because of increased charge traps due to adsorbed water. This is also seen on the bare hydrophilic surface which shows the lowest current and mobility. On the other hand, OTS showed better performance than the APTES, CTS, and bare surface, most likely due to its extreme hydrophobicity (less traps), despite poor transfers. Measurements were performed in a nitrogen environment free of water and oxygen to attribute the effect of adsorbed water. For all the SAMs, the on- and off-currents and mobility decreased, most likely due to the lack of oxygen which p-dopes the SWNTs, with the biggest change on the BTS surface. This may show that the other surfaces are more affected by the negative impact of water in air. The results are summarized in Figure S5 in Supporting Information.

The slight differences in V_t between the different SAMs can be attributed to the dipole moment and hydrophobicity of the SAM. This has previously been observed with organic field effect transistors.[26,27] In our study, OTS, the most hydrophobic surface, has the smallest V_t, most likely due to smallest amount of surface traps caused by adsorbed water. Measurements performed in the water-free environment showed a much narrower distribution of V_t in addition to all V_t shifting toward a more negative voltage, confirming the impact of adsorbed water (Figure S5 in Supporting Information). These results should be taken with caution, however, as V_t is a difficult parameter to analyze for SWNT films as it is additionally influenced by SWNT/electrode contact, SWNT/SWNT interactions,[37] and defects from the dielectric. The effect of the dipole moment on the V_t remains unclear. It is possible to
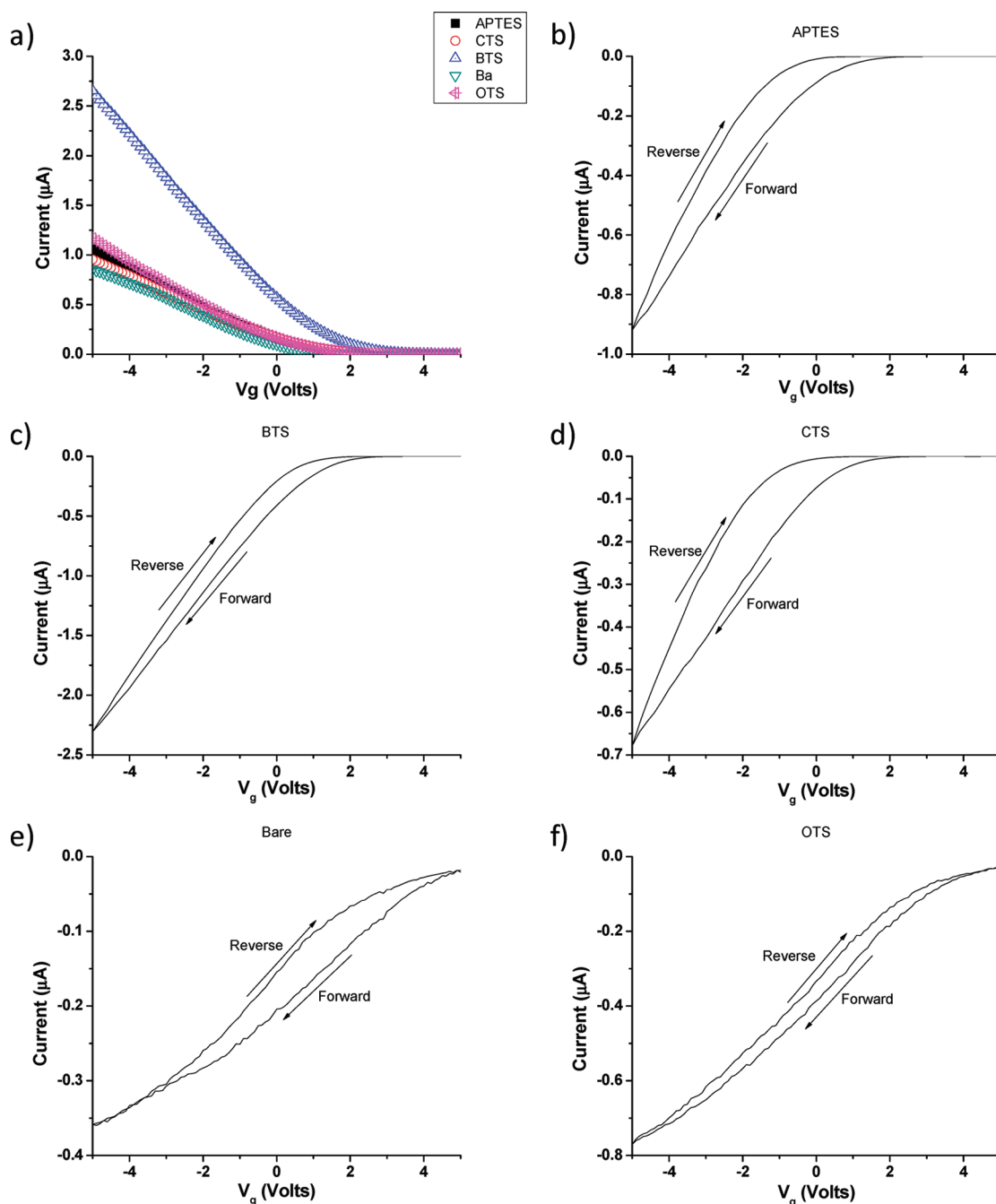
Figure 2. (a) Average transfer curves for transfer samples. Channel dimensions for transistor devices are L_c = 50 m and W_c = 1000 m; V_{ds} = −0.5 V. Typical hysteresis plots (one device) for (b) APTES, (c) BTS, (d) CTS, (e) bare, (f) OTS. Smallest hysteresis observed on OTS and BTS (most hydrophobic surfaces). APTES refers to transferred APTES surfaces.

calculate the dipole moment of the individual molecules composed in the SAM to compare with our results and understand what effect, if any, this may have. However, values obtained in this manner would not reflect SAM/substrate interaction and therefore can lead to inaccurate results. Although our results clearly indicate that substrate chemistry influences charge transport, a more rigorous model is currently being developed to calculate a more accurate theoretical value for the *surface* dipole moment to understand this contribution and is the subject of ongoing work.

Finally, a look at the hysteresis plots in Figure 2b−f between the different SAMs shows a smaller hysteresis for the surfaces with the BTS and OTS SAMs compared to other surfaces. It has been shown that adsorbed water is a major cause for hysteresis in SWNT FETs most likely due to charge trapping as mentioned before.[38] The lower hysteresis with OTS and BTS surfaces is consistent with the previous observation as they are more hydrophobic than the APTES, CTS, and bare SiO₂ surfaces. In addition, hysteresis measurements in the water-free environment showed lower hysteresis for
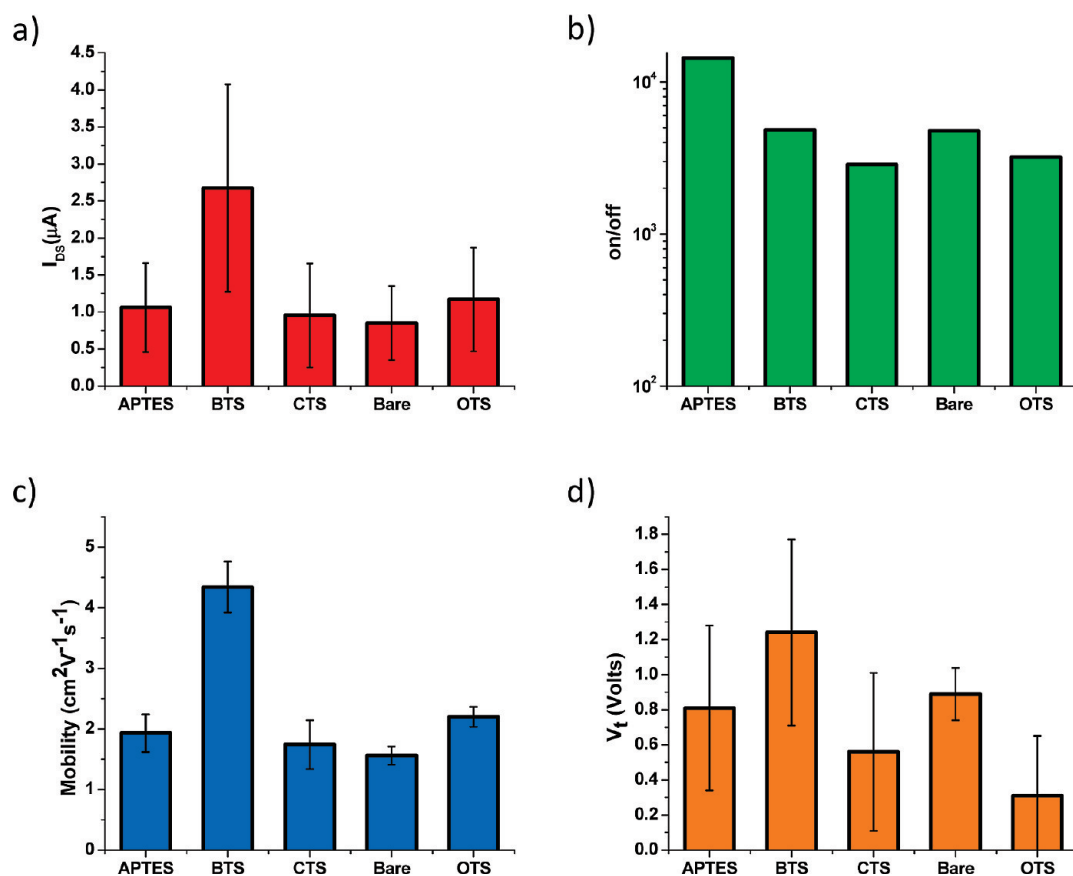
Figure 3. Summary of electrical properties of TFTs on different SAMs: (a) average source drain current at $V_g = -5$ V, (b) median on/off ratio (95% of devices above 10^3), (c) average field effect mobility, (d) average threshold voltage; $V_{ds} = -0.5$ V with $V_g = 5$ to -5 V for all data. APTES refers to transferred APTES surfaces.

the APTES, CTS, and bare SiO_2 surfaces, making them similar to the OTS and BTS surfaces and confirming the previous trend (Figure S6 in Supporting Information).

μ-Raman Analysis. μ-Raman spectroscopy was used to corroborate the conclusions drawn from the electrical data. Here, 1.96 eV laser was used as this energy is resonant with a large population of the SWNTs used in our experiments ($\sim 1.4 \pm 0.5$ nm). The radial breathing mode (RBM) region (typically in the range of $120-250$ cm^{-1}) can be used to determine the chirality of the nanotubes.[39,40] We did not see any major differences between different SAMs as expected in this region (Figure 4a,c), which confirmed that the chirality was not changing during transfer. In other words, no selective transfer depending on chirality was observed. In addition, we saw a slight quenching on the bare and BTS surfaces and a slight enhancement on the CTS and APTES surfaces (Figure 4a), which is consistent with previous reports of p-doping and n-doping of SWNTs, respectively.[39] The G band region (typically in the rage of $1550-1605$ cm^{-1}) can be used to distinguish between metallic and semiconducting tubes. It is composed of two intense peaks which are due to vibrations along the tube axis (G^+) and vibrations in the circumferential direction (G^-). The G^- peak has a Lorentzian line shape for semiconductor SWNTs and a broad Breit−Wigner−Fano line shape for metallic

SWNTs.[40,41] In addition, it has been shown that dopants not only change the line shape from one to the other but also shift the location of the G^- peak.[42] As a result, we can use the G^- peak to qualitatively analyze the effect of the SAMs on the primarily semiconducting SWNTs on our surfaces. Figure 4b shows overlaid plots of the G band region for the different SAMs. Rao *et al.* have shown that doping SWNTs with an electron-withdrawing group, such as bromine, upshifts the G^- peak, whereas doping with electron-donating groups downshifts it. We observed the same trends with our SAMs. This indicates that there may be charge transfer taking place between the SAMs and the SWNTs. Figure 4d shows the full width half-maximum (fwhm) of the entire G band (G^- and G^+), and as expected, BTS had the smallest value while the electron-donating APTES had the largest value. Figure 4d shows the D/G ratios of the different surfaces. The D band has been associated with the disorder in the SWNTs. The D/G ratios can be used as a semiquantitative method to determine the level of defects.[43] We did not see any damage done during the transfer process, as the D/G ratio was within normal limits of $0.2-0.3$ (typical values we have observed before) for all our samples.

In conclusion, we have utilized a dry transfer method that could transfer intact SWNT networks on many different surfaces. Using this technique, organized net-
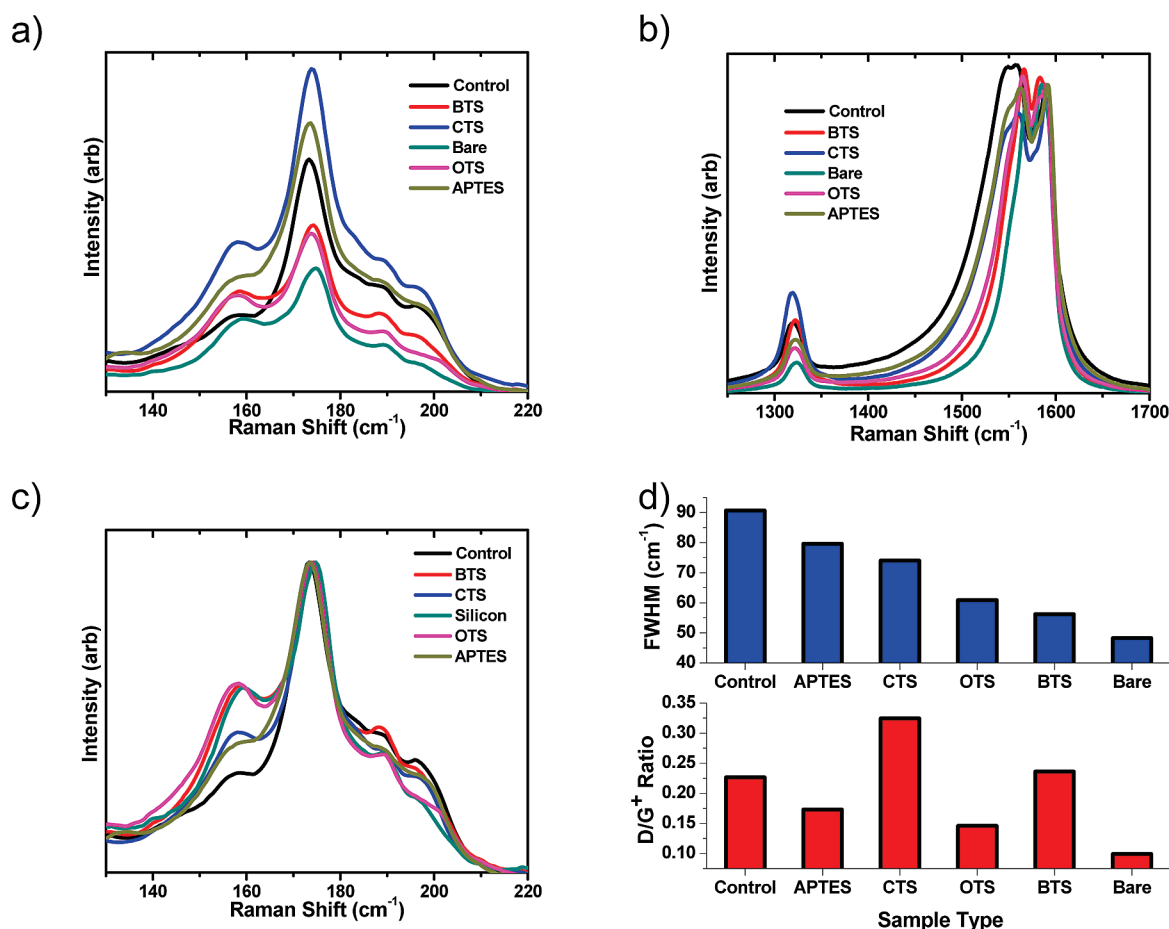
Figure 4. μ-Raman data summary. (a) RBM region normalized for silicon peak intensity (303 nm) showing that RBM is quenched for BTS and bare surfaces. (b) Normalized G and D bands for different SAMs. (c) Normalized RBM for different SAMs showing that there is no chirality changing upon transfer to different surfaces. (d) Fwhm and D/G ratios. The fwhm decreases with level of doping. APTES refers to transferred APTES surfaces and control refers to original APTES surfaces before transfer.

works can be fabricated on surfaces not before possible from solution. We have shown that SAMs have a significant impact on the electrical properties of carbon nanotubes and thus can be used to tune device properties despite the small area of interaction. Especially important are the functional groups of the SAM and their electron-donating/withdrawing properties. This can help to unravel fundamental insight into SWNT elec-

tronic properties and to develop tunable SWNT networks that can enable more reliable transistors and sensors. More work can be done to investigate other properties of the SAMs, such as hydrophobicity and other functional groups. There is a myriad of SAMs that can be investigated and potentially can give more insight or other interesting changes in SWNT-based devices.

MATERIALS AND METHODS

Surface Preparation. Doped silicon wafers with (100) surface (Silicon Quest) with 300 nm are cut into 2.5 × 1 cm pieces and cleaned using Piranha solution (3:1 H_2SO_4/H_2O_2). After Piranha cleaning, the wafers were washed with deionized water and dried using a N_2 gun. All silanes were purchased from Gelest. APTES and CTS SAMs were made inside a glovebox (N_2 environment) and in anhydrous toluene (0.4 and 1% by volume, respectively), due to water sensitivity. BTS (1% by volume) SAMs were made in ambient air using regular toluene. APTES, CTS, and BTS were reacted for 1, 2, and 24 h, respectively. The OTS surface was made using a method we reported to prepare highly dense OTS SAMs.[44] After reaction, the wafers were rinsed twice with toluene and then bath sonicated in toluene for 2 min to remove any multilayers. Then, they were N_2 dried and annealed under vacuum for 20 min at 90−100 °C. Top contact electrodes were deposited from 40 nm gold through a shadow mask.

Nanotube Solution Preparation. Arc-discharge nanotubes were sonicated in NMP at 30% power for 30 min. The solution was then centrifuged for 1.5 h at 15 000 rpm to remove bundles, amorphous carbon, or other contaminants. The final solution had a concentration of about 10 μg/mL.

Spin-Coating on APTES. A total of 150 μL (10 μL at a time) of solution was dropped using a pipet at the center of the wafer while it was spinning at 4000 rpm in air.

Transfer Printing. Sixty nanometers of gold was evaporated on top of the SWNT films on the APTES SAM to aid in the transfer process. Thermal adhesive tape (Revalpha, Nitto Denko) was pressed lightly on the gold and peeled off, removing the gold/SWNT film. This was then pressed firmly on the target substrate and heated to 120 °C, at which time the thermal adhesive tape lost adhesion and was released. The gold was then etched by placing in a potassium iodide gold etchant solution (GE-8110,

Transene) for 45 min. After etching, the surfaces were washed with water and dried with N_2.

Characterization. AFM images were taken using tapping mode (light tapping regime) using a Multimode AFM (Veeco). Electrical testing was done using Keithley 4200 SC semiconductor analyzer. μ-Raman (LabRam Aramis, Horiba Jobin Yvon) measurements were carried at 633 nm (1.96ev) excitation at 100× magnification, 1 μm spot size, and 1800 grating. Excitation power was 2 mV. Data were taken using an automated multi-point mapping (6 points) between the channels (3 different channels per sample). The spectra were then averaged for each sample and normalized to the 303 cm^{-1} silicon peak.

Transistor Calculations. Top gate configuration is used with heavily doped silicon as the back gate and 300 nm SiO_2 as the dielectric. Source−drain current (I_{ds}) was measured by sweeping the gate voltage (V_g) from −5 to 5 V at a source−drain voltage (V_{ds}) of −0.5 V. On-current (I_{on}) was determined at $V_g = -5$ V. On/off ratio was determined by taking the ratio of I_{on} to I_{off}, where I_{off} is determined by averaging the I_{ds} at $V_g = 4.8-5.0$ V. Mobility (μ) and threshold voltage (V_t) values were calculated using the linear transistor equation ($I_{ds} = (WC\mu/L) \times (V_g - V_t - V_{ds}/2) \times V_{ds})$) as we are operating in the linear regime since $V_{ds} \ll V_g$.[45] A capacitance value of 1.0×10^{-8} F/cm^2 was obtained using a simple parallel plate model. A more rigorous model taking into account capacitance coupling of the SWNTs can be used:[46]

$$C = \left\{ C_Q^{-1} + \frac{1}{2\pi\varepsilon_0\varepsilon_{ox}}\ln\left[\frac{\Lambda_0 \sin h(2\pi t_{ox}/\Lambda_0)}{R\pi}\right]\right\}^{-1}\Lambda_0^{-1}$$

where $1/\Lambda_0$ is the density of nanotubes and is approximated to be ∼9 tubes/μm by AFM, $C_Q = 4.0 \times 10^{-10}$ F/m and is the quantum capacitance of nanotubes, $t_{ox} = 300$ nm is the oxide thickness, $R = 1.5$ nm is the average tube diameter, and $\varepsilon_0\varepsilon_{ox} = 3.9 \times 8.85 \times 10^{-14}$ F/cm is the dielectric constant at the interface. Using this model, a capacitance value of 9.7×10^{-7} F/cm^2 is obtained. Since both values are almost identical, an approximate capacitance of 1.0×10^{-8} F/cm^2 was used for mobility calculations.

Supporting Information Available: AFM images of bare surfaces and surfaces during transfer process, output curves, and electrical data in N_2 environment (free of water and oxygen). This material is available free of charge *via* the Internet at http://pubs.acs.org.

REFERENCES AND NOTES

1. Baughman, R. H.; Zakhidov, A. A.; de Heer, W. A. Carbon Nanotubes—The Route toward Applications. *Science* **2002**, *297*, 787–792.
2. Hu, J.; Odom, T. W.; Lieber, C. M. Chemistry and Physics in One Dimension: Synthesis and Properties of Nanowires and Nanotubes. *Acc. Chem. Res.* **1999**, *32*, 435–445.
3. Ahn, J. H.; Kim, H. S.; Lee, K. J.; Jeon, S.; Kang, S. J.; Sun, Y.; Nuzzo, R. G.; Rogers, J. A. Heterogeneous Three-Dimensional Electronics by Use of Printed Semiconductor Nanomaterials. *Science* **2006**, *314*, 1754–1757.
4. Gruner, G. Carbon Nanotube Films for Transparent and Plastic Electronics. *J. Mater. Chem.* **2006**, *16*, 3533–3539.
5. Rowell, M. W.; Topinka, M. A.; McGehee, M. D.; Prall, H.-J.; Dennler, G.; Sariciftci, N. S.; Hu, L.; Gruner, G. Organic Solar Cells with Carbon Nanotube Network Electrodes. *Appl. Phys. Lett.* **2006**, *88*, 233506-1–233506-3.
6. Roberts, M. E.; LeMieux, M. C.; Bao, Z. Sorted and Aligned Single-Walled Carbon Nanotube Networks for Transistor-Based Aqueous Chemical Sensors. *ACS Nano* **2009**, *3*, 3287–3293.
7. Star, A.; Han, T.-R.; Gabriel, J.-C. P.; Bradley, K.; Gruner, G. Interaction of Aromatic Compounds with Carbon Nanotubes: Correlation to the Hammett Parameter of the Substituent and Measured Carbon Nanotube FET Response. *Nano Lett.* **2003**, *3*, 1421–1423.
8. Novak, J. P.; Snow, E. S.; Houser, E. J.; Park, D.; Stepnowski, J. L.; McGill, R. A. Nerve Agent Detection Using Networks of Single-Walled Carbon Nanotubes. *Appl. Phys. Lett.* **2003**, *83*, 4026–4028.
9. Lee, C. Y.; Strano, M. S. Understanding the Dynamics of Signal Transduction for Adsorption of Gases and Vapors on Carbon Nanotube Sensors. *Langmuir* **2005**, *21*, 5192–5196.
10. Wang, F.; Gu, H.; Swager, T. M. Carbon Nanotube/Polythiophene Chemiresistive Sensors for Chemical Warfare Agents. *J. Am. Chem. Soc.* **2008**, *130*, 5392–5393.
11. Huang, L.; Jia, Z.; O'Brien, S. Oriented Assembly of Single-Walled Carbon Nanotubes and Applications. *J. Mater. Chem.* **2007**, *17*, 3863–3874.
12. Avouris, P.; Chem, Z.; Perebeinos, V. Carbon-Based Electronics. *Nat. Nanotechnol.* **2007**, *2*, 605–615.
13. Li, Y.; Mann, D.; Rolandi, M.; Kim, W.; Ural, A.; Hung, S.; Javey, A.; Cao, J.; Wang, D.; Yenilmez, E.; Wang, Q.; Gibbons, J. F.; Nishi, Y.; Dai, H. Preferential Growth of Semiconducting Single-Walled Carbon Nanotubes by a Plasma Enhanced CVD Method. *Nano Lett.* **2004**, *4*, 317–321.
14. Strano, M. S. Carbon Nanotubes: Sorting out Left from Right. *Nat. Nanotechnol.* **2007**, *2*, 340–341.
15. Arnold, M. S.; Green, A. A.; Hulvat, J. F.; Stupp, S. I.; Hersam, M. C. Sorting Carbon Nanotubes by Electronic Structure Using Density Differentiation. *Nat. Nanotechnol.* **2006**, *1*, 60–65.
16. Buldum, A.; Lu, J. P. Contact Resistance between Carbon Nanotubes. *Phys. Rev. B* **2001**, *63*, 161403-1–161403-4.
17. Fuhrer, M. S.; Nygrd, J.; Shih, L.; Forero, M.; Yoon, Y.-G.; Mazzoni, M. S. C.; Choi, H. J.; Ihm, J.; Louie, S. G.; Zettl, A.; McEuen, P. L. Crossed Nanotube Junctions. *Science* **2000**, *288*, 494–497.
18. Cao, Q.; Rogers, J. A. Ultrathin Films of Single-Walled Carbon Nanotubes for Electronics and Sensors: A Review of Fundamental and Applied Aspects. *Adv. Mater.* **2009**, *21*, 29–53.
19. Kocabas, C.; Hur, S. H.; Gaur, A.; Meitl, M. A.; Shim, M.; Rogers, J. A. Guided Growth of Large-Scale, Horizontally Aligned Arrays of Single-Walled Carbon Nanotubes and Their Use in Thin-Film Transistors. *Small* **2005**, *1*, 1110–1116.
20. Krupke, R.; Hennrich, F.; Loehneysen, H. V.; Kappes, M. M. Separation of Metallic from Semiconducting Single-Walled Carbon Nanotubes. *Science* **2003**, *301*, 344–347.
21. Rao, S. G.; Huang, L.; Setyawan, W.; Hong, S. Nanotube Electronics: Large-Scale Assembly of Carbon Nanotubes. *Nature* **2003**, *425*, 36–37.
22. Li, X.; Zhang, L.; Wang, X.; Shimoyama, I.; Sun, X.; Seo, W. S.; Dai, H. Langmuir−Blodgett Assembly of Densely Aligned Single-Walled Carbon Nanotubes from Bulk Materials. *J. Am. Chem. Soc.* **2007**, *129*, 4890–4891.
23. LeMieux, M. C.; Roberts, M.; Barman, S.; Jin, Y. W.; Kim, J. M.; Bao, Z. Self-Sorted, Aligned Nanotube Networks for Thin-Film Transistors. *Science* **2008**, *321*, 101–104.
24. Roberts, M. E.; LeMieux, M. C.; Sokolov, A. N.; Bao, Z. Self-Sorted Nanotube Networks on Polymer Dielectrics for Low-Voltage Thin-Film Transistors. *Nano Lett.* **2009**, *9*, 2526–2531.
25. Opatkiewicz, J. P.; LeMieux, M. C.; Bao, Z. Influence of Electrostatic Interactions on Spin-Assembled Single-Walled Carbon Nanotube Networks on Amine-Functionalized Surfaces. *ACS Nano* **2010**, *4*, 1167–1177.
26. Possanner, S. K.; Zojer, K.; Pacher, P.; Zojer, E.; Schurrer, F. Threshold Voltage Shifts in Organic Thin-Film Transistors Due to Self-Assembled Monolayers at the Dielectric Surface. *Adv. Funct. Mater.* **2009**, *19*, 958–967.
27. Pernstich, K. P.; Haas, S.; Oberhoff, D.; Goldmann, C.; Gundlach, D. J.; Batlogg, B.; Rashid, A. N.; Schitter, G.

Threshold Voltage Shift in Organic Field Effect Transistors by Dipole Monolayers on the Gate Insulator. *J. Appl. Phys.* **2004**, *96*, 6431–6438.

28. Kim, W.; Javey, A.; Vermesh, O.; Wang, Q.; Li, Y.; Dai, H. Hysteresis Caused by Water Molecules in Carbon Nanotube Field-Effect Transistors. *Nano Lett.* **2003**, *3*, 193–198.

29. Koboyashi, S.; Nishikawa, T.; Takenobu, T.; Mori, S.; Shimoda, T.; Mitani, T.; Shimotani, H.; Yoshimoto, N.; Ogawa, S.; Iwasa, T. Control of Carrier Density by Self-Assembled Monolayers in Organic Field-Effect Transistors. *Nat. Mater.* **2004**, *3*, 317–322.

30. Hur, S.-H.; Yoon, M.-H.; Gaur, A.; Shim, M.; Facchetti, A.; Marks, T. J.; Rogers, J. A. Organic Nanodielectrics for Low Voltage Carbon Nanotube Thin Film Transistors and Complementary Logic Gates. *J. Am. Chem. Soc.* **2005**, *127*, 13808–13809.

31. Lee, R. S.; Kim, H. J.; Fischer, J. E.; Thess, A.; Smalley, R. E. Conductivity Enhancement in Single-Walled Carbon Nanotube Bundles Doped with K and Br. *Nature* **1997**, *388*, 255–257.

32. LeMieux, M. C.; Sok, S.; Roberts, M. E.; Opatkiewicz, J. P.; Liu, D.; Barman, S. N.; Patil, N.; Mitra, S.; Bao, Z. Solution Assembly of Organized Carbon Nanotube Networks for Thin-Film Transistors. *ACS Nano* **2009**, *3*, 4089–4097.

33. Zhou, Y.; Hu, L.; Gruner, G. A Method of Printing Carbon Nanotube Thin Films. *Appl. Phys. Lett.* **2006**, *88*, 123109-1–123109-3.

34. Kang, S. J.; Kocabas, C.; Kim, H. S.; Cao, Q.; Meitl, M. A.; Khang, D. Y.; Rogers, J. A. Printed Multilayer Superstructures of Aligned Single-Walled Carbon Nanotubes for Electronic Applications. *Nano Lett.* **2007**, *7*, 3343–3348.

35. Ding, L.; Tselev, A.; Wang, J.; Yuan, D.; Chu, H.; McNicholas, T. P.; Li, Y.; Liu, J. Selective Growth of Well-Aligned Semiconducting Single-Walled Carbon Nanotubes. *Nano Lett.* **2009**, *9*, 800–805.

36. Tabata, H.; Shimizu, M.; Ishibashi, K. Fabrication of Single Electron Transistors Using Transfer-Printed Aligned Single Walled Carbon Nanotube Arrays. *Appl. Phys. Lett.* **2009**, *95*, 113107-1–113107-3.

37. Engel, M.; Small, J. P.; Steiner, M.; Freitag, M.; Green, A. A.; Hersam, M. C.; Avouris, P. Thin Film Nanotube Transistors Based on Self-Assembled, Aligned, Semiconducting Carbon Nanotube Arrays. *ACS Nano* **2008**, *2*, 2445–2452.

38. Kim, W.; Javey, A.; Vermesh, O.; Wang, Q.; Li, Y.; Dai, H. Hysteresis Caused by Water Molecules in Carbon Nanotube Field-Effect Transistors. *Nano Lett.* **2003**, *3*, 193–198.

39. Zhou, W.; Nemes, N. M.; Fischer, J. E.; Borondics, F.; Kamaras, K.; Tanner, D. B. Charge Transfer and Fermi Level Shift in p-Doped Single-Walled Carbon Nanotubes. *Phys. Rev. B* **2005**, *71*, 205423-1–205423-7.

40. Jorio, A.; Saito, R.; Hafner, J. H.; Lieber, C. M.; Hunter, M.; McClure, T.; Dresselhaus, G.; Dresselhaus, M. S. Structural (*n,m*) Determination of Isolated Single-Wall Carbon Nanotubes by Resonant Raman Scattering. *Phys. Rev. Lett.* **2001**, *86*, 1118–1121.

41. Dresselhaus, M. S.; Dresselhaus, G.; Jorio, A.; Souza Filho, A. G.; Saito, R. Raman Spectroscopy on Isolated Single Wall Carbon Nanotubes. *Carbon* **2002**, *40*, 2043–2061.

42. Rao, A. M.; Eklund, P. C.; Bandow, S.; Thess, A.; Smalley, R. E. Evidence of Charge Transfer in Doped Carbon Nanotube Bundles from Raman Scattering. *Nature* **1997**, *388*, 257–259.

43. Lucchese, M. M.; Stavale, F.; Ferreira, E. H.; Vilane, C.; Moutinho, M. V. O.; Capaz, R. B.; Achete, C. A.; Jorio, A. Quantifying Ion-Induced Defects and Raman Relaxation Length in Graphene. *Carbon* **2010**, *48*, 1592–1597.

44. Ito, Y.; Virkar, A. A.; Mannsfeld, S.; Oh, J. H.; Toney, M.; Locklin, J.; Bao, Z. Crystalline Ultrasmooth Self-Assembled Monolayers of Alkylsilanes for Organic Field-Effect Transistors. *J. Am. Chem. Soc.* **2009**, *131*, 9396–9404.

45. Dimitrakopoulos, C. D.; Malenfont, R. L. Organic Thin Film Transistors for Large Area Electronics. *Adv. Mater.* **2002**, *14*, 99–117.

46. Wang, C.; Zhang, J.; Ryu, K.; Badmaev, A.; De Arco, L. G.; Zhou, C. Wafer-Scale Fabrication of Separated Carbon Nanotube Thin-Film Transistors for Display Applications. *Nano Lett.* **2009**, *9*, 4285–4291.